



# $P_{1-x}Ta_{8+x}N_{13}$ ( $x=0.1-0.15$ ): A Phosphorus Tantalum Nitride Featuring Mixed-Valent Tantalum and P/Ta Disorder Visualized by Scanning Transmission Electron Microscopy

Monika M. Pointner, Claude Ceniza, Lukas Nusser, Kristian Witthaut, Florian Wolf, Martin Weidemann, Lucien Eisenburger, Alexander Moewes, Oliver Oeckler,\* and Wolfgang Schnick\*

**Abstract:** We report on the synthesis, crystal, and electronic structure, as well as the magnetic, and electric properties of the phosphorus-containing tantalum nitride  $P_{1-x}Ta_{8+x}N_{13}$  ( $x=0.1-0.15$ ). A high-pressure high-temperature reaction (8 GPa, 1400 °C) of  $Ta_3N_5$  and  $P_3N_5$  with  $NH_4F$  as a mineralizing agent yields the compound in the form of black, rod-shaped crystals. Single-crystal X-ray structure elucidation (space group  $C2/m$  (no. 12),  $a=16.202(3)$ ,  $b=2.9155(4)$ ,  $c=11.089(2)$  Å,  $\beta=126.698(7)^\circ$ ,  $Z=2$ ) shows a network of face- and edge-sharing Ta-centered polyhedra that contains small vacant channels and  $PN_6$  octahedra strands. Atomic resolution transmission electron microscopy reveals an unusual P/Ta disorder. Mixed-valent tantalum atoms exhibit interatomic distances similar to those in metallic tantalum, however, the electrical resistivity is quite high in the order of  $10^1 \Omega\text{cm}$ . The density of states and the electron localization function indicate localized electrons in both covalent and ionic bonds between P/Ta and N atoms, combined with less localized electrons that do not contribute to interatomic bonds.

Transition metal (TM) nitrides and ternary metal nitrides have become an integral part of today's electrochemical energy applications and fundamental research projects because they offer a versatile range of desirable properties for sustainable energy conversion, including photovoltaics, thermoelectric materials, and solid-state lighting.<sup>[1-2]</sup> Tantalum nitrides exhibit properties like tunable electrical conductivity ideal for applications in, e.g., microelectronics, solar energy harvesting, and catalysis.<sup>[3-5]</sup> The Ta–N system spans a spectrum from tantalum-rich solid solutions to nitrogen-rich compounds with varying oxidation states from 0 to +V. Known phases include the solid solution of nitrogen in tantalum,<sup>[6]</sup>  $\alpha$ -Ta(N) and  $\beta$ -Ta<sub>2</sub>N,<sup>[6-9]</sup> three modifications of TaN ( $\epsilon$ ,  $\delta$ ,  $\theta$ ),<sup>[9-15]</sup> as well as nitrogen-rich compounds like Ta<sub>5</sub>N<sub>6</sub>,<sup>[7]</sup> Ta<sub>4</sub>N<sub>5</sub>,<sup>[7]</sup> Ta<sub>2</sub>N<sub>3</sub>,<sup>[16-17]</sup> and Ta<sub>3</sub>N<sub>5</sub>.<sup>[18]</sup> The binary system Ta–N is so intriguing that calculations are being made to explore the less accessible high-pressure/high-temperature Ta–N phase diagram.<sup>[19]</sup>

Ternary compounds with Ta and N form nitridotantalates with discrete or vertex-sharing Ta<sup>+V</sup>N<sub>4</sub> tetrahedra, as well as Ta<sup>+V</sup>N<sub>6</sub> octahedra if alkaline and alkaline earth metals are included.<sup>[20-24]</sup> Nitridotantalates like LiTa<sub>3</sub>N<sub>4</sub>, MgTa<sub>2</sub>N<sub>3</sub>, Na<sub>2</sub>Ta<sub>3</sub>N<sub>5</sub> and Na<sub>x</sub>Ta<sub>3</sub>N<sub>5</sub> ( $0 \leq x \leq 1.4$ ) show mixed-valency of the Ta species.<sup>[25-26]</sup> The systems Ta/TM/N were studied in detail in the mid 20th century and it was shown that compounds with  $TM=Ti-Ni$ ,  $Zr-Nb$  typically form disordered rock salt-type structures.<sup>[9,12,27]</sup> With copper as a second TM, CuTa<sub>2</sub>N<sub>2</sub> forms a layered delafossite-type structure with Ta<sup>+V</sup>N<sub>6</sub> octahedra.<sup>[28]</sup> Recently discovered MnTa<sub>2</sub>N<sub>4</sub> and ScTa<sub>2</sub>N<sub>2</sub>, feature pronounced magnetic frustration and metal–metal bonds, respectively.<sup>[29-30]</sup> A handful of ternary Ta–N compounds involve rare-earth metals.  $RE_3[Ta_2N_6]$  ( $RE=La, Ce, Pr$ ) are isotypic to the high  $T_C$  cuprate semiconductor La<sub>2-x</sub>Sr<sub>x</sub>CaCu<sub>2</sub>O<sub>6</sub> ( $x=0.2-0.55$ ) and contain layers of vertex-sharing square TaN<sub>5</sub> pyramids.<sup>[31]</sup> TaThN<sub>3</sub> was the first nitride perovskite in literature.<sup>[32]</sup> For the main group elements from groups 13 to 15, Ta<sub>5</sub>Ga<sub>3</sub>N forms a typical 5/3-intermetallic structure with interstitial N, and tantalum carbonitrides have been reported due to the solubility of TaN in C.<sup>[12,33-34]</sup>

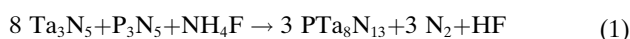
The introduction of phosphorus into TM nitrides led to anionic nitridophosphate network systems dominated by PN<sub>4</sub> tetrahedra<sup>[35-36]</sup> and TM nitrides containing phosphorus,

[\*] M.Sc. M. M. Pointner, M.Sc. L. Nusser, M.Sc. K. Witthaut, M.Sc. F. Wolf, M.Sc. M. Weidemann, Dr. L. Eisenburger, Prof. Dr. W. Schnick  
Department of Chemistry  
University of Munich (LMU)  
Butenandtstraße 5–13, 81377 Munich, Germany  
E-mail: wolfgang.schnick@uni-muenchen.de  
B.Sc. C. Ceniza, Prof. Dr. A. Moewes  
Department of Physics and Engineering Physics  
University of Saskatchewan  
116 Science Place, Saskatoon, Saskatchewan, S7N 5E2, Canada  
Prof. Dr. O. Oeckler  
Institute for Inorganic Chemistry and Crystallography  
Leipzig University  
Scharnhorststraße 20, 04275 Leipzig, Germany  
E-mail: oliver.oeckler@gmx.de

© 2024 The Authors. Angewandte Chemie International Edition published by Wiley-VCH GmbH. This is an open access article under the terms of the Creative Commons Attribution Non-Commercial NoDerivs License, which permits use and distribution in any medium, provided the original work is properly cited, the use is non-commercial and no modifications or adaptations are made.

which are mostly unexplored. Therefore, we search for possible synthesis routes and structure–property relationships. In this article, we present  $P_{1-x}Ta_{8+x}N_{13}$  ( $x=0.1-0.15$ ), a ternary transition metal nitride that combines occupational disorder of Ta and P, mixed-valence tantalum with a formal oxidation state of +4.25 and  $PN_6$  octahedra, a structure motif typically found in high-pressure chemistry within pressure ranges achieved by diamond anvil cells.<sup>[37–39]</sup>

The title compound was obtained at high-pressure high-temperature conditions ( $T=1400^\circ\text{C}$ ,  $p=8\text{ GPa}$ ) from the respective binary nitrides  $Ta_3N_5$  and  $P_3N_5$ , using excess  $P_3N_5$  and 1 eq.  $NH_4F$  as a mineralizing agent. It is assumed that the synthesis follows the reaction equation (1), in which the surplus and the mixed occupation are not accounted for. Further details on the multi-anvil setup can be found in the Experimental Section in the Supporting Information.



The reaction yields a black microcrystalline powder, which is stable toward air and moisture. The rod-shaped crystals are around  $2\ \mu\text{m}$  in width and up to  $10\ \mu\text{m}$  in length (Figures 1 and S1). The crystal structure of  $P_{1-x}Ta_{8+x}N_{13}$  ( $x=0.1-0.15$ ) is obtained from single-crystal X-ray diffraction (SCXRD) data resulting in the monoclinic space group  $C2/m$  (no. 12) with  $a=16.202(3)\ \text{\AA}$ ,  $b=2.9155(4)\ \text{\AA}$ ,  $c=11.089(2)\ \text{\AA}$ ,  $\beta=126.698(7)^\circ$  and  $Z=2$  ( $RI=0.0586$ ,  $wR2=0.1418$ ,  $R_g=0.0730$ ,  $GoF=1.094$ ). Further details and crystallographic data can be found in the Supporting Information. A tilt series of selected area electron diffraction (SAED) patterns matches the simulations and confirms the metric of the unit cell (Figure S2). Rietveld refinements on powder X-ray diffraction (PXRD) data were used to analyze the phase composition (Figure S4). Only small amounts of unknown side phases are present, which could be of a P-rich nature due to the excess of P in the synthesis. With transmission and scanning electron microscopy no crystalline side phases could be identified and there are no indications of amorphous side phases. Amorphization of  $P_3N_5$  could not be observed. High-temperature PXRD demonstrates stability up to at least  $900^\circ\text{C}$  in air and reveals a thermal expansion of less than 15% of the cell volume up to  $900^\circ\text{C}$  (Figure S5). The elemental composition was analyzed by energy dispersive X-ray spectroscopy (EDX)

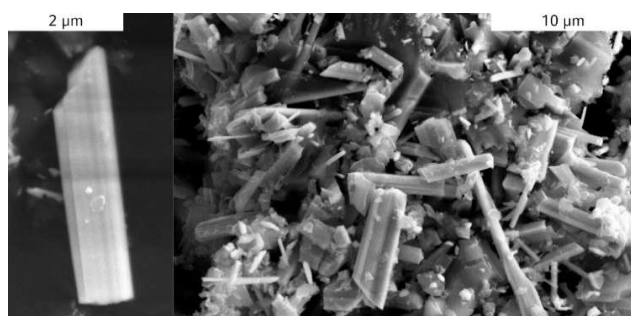


**Figure 1.** Secondary electron image of crystals of  $P_{1-x}Ta_{8+x}N_{13}$  ( $x=0.1-0.15$ ). Crystals are around  $2\ \mu\text{m}$  in width and up to  $10\ \mu\text{m}$  in length.

and indicates a minor amount of oxygen (Table S7). This is in line with reports that tantalum nitrides are very susceptible for oxygen impurities.<sup>[40–41]</sup> Since slight fluctuations in the composition variations cannot be ruled out, a variation or range in stoichiometric formula of  $P_{1-x}Ta_{8+x}N_{13-y}O_y$  ( $x=0.1-0.15$ ,  $y\leq 1$ ) could be considered.

The structure of  $P_{1-x}Ta_{8+x}N_{13}$  ( $x=0.1-0.15$ ) can be described as a network of face- and edge-sharing Ta-centered polyhedra. Both edge-sharing P-centered octahedra and small vacant channels extend along  $[010]$  (Figure 2). The structure shows a certain similarity with the high-pressure polymorph  $Ta_3N_5$  ( $Pnma$ ,  $U_3Te_5$  structure type, Figure S6). Both structures exhibit a similar condensed network with vacant channels and a short  $b$  lattice parameter that corresponds to a Ta-centered polyhedron ( $P_{1-x}Ta_{8+x}N_{13}$ :  $2.9155(4)\ \text{\AA}$ ,  $HP-Ta_3N_5$ :  $2.691(5)\ \text{\AA}$ ).

Four crystallographically distinct Ta sites are seven or eightfold coordinated by nitrogen. Ta2 and Ta3 form capped trigonal prisms (CN=7) and Ta4 as well as Ta5 form bicapped trigonal prisms (CN=8). Ta–N distances (Ta2–Ta5) range from  $2.10(5)\ \text{\AA}$  to  $2.49(4)\ \text{\AA}$  and agree with other tantalum nitrides.<sup>[7,9,18]</sup> Trigonal prisms are a well-known coordination motif in binary and ternary tantalum nitrides and capped versions have also been observed in high-pressure phases such as  $Ta_3N_5$  ( $Pnma$ ) and  $\eta-Ta_2N_3$ .<sup>[17]</sup> All coordination polyhedra are shown in Figure S7.

$PN_6$  octahedra have common edges along  $[010]$ . The phosphorus site exhibits a mixed occupancy of  $P_{1-x}$  and  $Ta_x$  with  $x=0.1-0.15$  as derived from single-crystal data. P–N distances range from  $1.78(4)\ \text{\AA}$  to  $1.94(3)\ \text{\AA}$ , with the average being slightly larger than other phases with  $PN_6$  octahedra, e.g.,  $\beta-BP_3N_6$  with  $d(P-N)=1.81(4)\ \text{\AA}$  at ambient pressure.<sup>[39]</sup> The mixed occupancy of P and Ta is most likely the reason for this increase. A formal consideration of the ionic radii of  $Ta^{+V}$  (64 pm) and  $P^{+V}$  (38 pm) indicates that the tantalum atoms are almost double in size, which significantly expands the volumes of the octahedra.<sup>[42]</sup> The structural motif of a  $PN_6$  octahedron is characteristic of high-pressure phases obtained in diamond anvil cells ( $\sim 40-140\text{ GPa}$ ).<sup>[37–39]</sup>  $P_{1-x}Ta_{8+x}N_{13}$  ( $x=0.1-0.15$ ) demonstrates that a suitable network enables the stabilization of this characteristic high-pressure motif even at significantly lower pressures ( $< 20\text{ GPa}$ ).

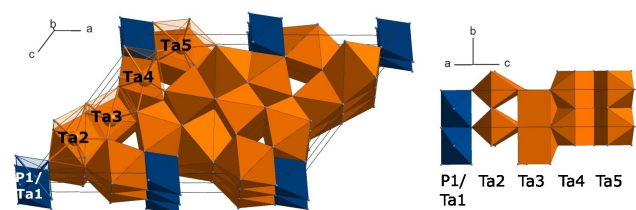


**Figure 2.** The crystal structure consists of a three-dimensional network of  $TaN_7$  and  $TaN_8$  polyhedra (orange) and  $(P/Ta)N_6$  octahedra (blue). Left: Two unit cells stacked along  $[010]$ . Right: Section through unit cell showing edge- (Ta2) and face-sharing (Ta3–Ta5) Ta-centered polyhedra along  $[010]$ . Some atomic sites are labeled.

The structure model has been validated by scanning transmission electron microscopy high-angle annular dark-field (STEM-HAADF) images with a Z-contrast according to  $Z^2$  ( $Z_P=15$ ,  $Z_{Ta}=73$ ).<sup>[43]</sup> STEM-HAADF images along [010] show uniform intensity for all Ta positions and positions with almost no intensity. The latter can be assigned to the P site by an atomic resolution EDX map (Figure 3a). The occupational disorder of Ta and P is clearly visible whenever high intensity of Ta occupies the P site. An explicit intensity profile of the EDX map shows that P positions occupied by Ta experience a clear loss of P-EDX signal and an increase in Ta-EDX signal (Figure 3b). Three different magnifications indicate that the disorder occurs throughout the entire crystal (Figure 3c).

Temperature dependent electrical resistivity at higher temperatures shows a linear behavior typical for metals. At lower temperatures the signal is dominated by impurities or defects in the material and becomes almost constant with temperature. The resistivity is in the order of  $10^{-1} \Omega\text{cm}$  (Figure 4a), much higher than conventional metals with a resistivity of  $\sim 10^{-8} \Omega\text{cm}$ , but shows similarities to that of some divalent transition metal oxides, e.g., Magnéli type oxides.<sup>[44]</sup> Distances between tantalum atoms (2.9155(5)–3.099(5) Å) are short and in the range of Ta–Ta bonds known from metallic tantalum and  $\vartheta$ - or  $\varepsilon$ -TaN (2.86–2.91 Å). The conductivity probably originates from the few

5d electrons of Ta that do not contribute to covalent Ta–N bonds. A diffuse reflectance spectrum shows strong optical absorption in the near IR that is due to excitable states around the Fermi-level, which corroborates the metallic character (Figure S12).

Magnetic susceptibility shows paramagnetic behavior down to 2.1 K with an effective magnetic moment of  $2.41(2) \mu_B$  per formula unit obtained from a Curie Weiss fit of the inverse molar susceptibility (Figure S13). The magnetization isotherm shows no sign of superconducting or ferromagnetic impurities (Figure S14). The EPR spectrum lacks distinct features, indicating the absence of unpaired electrons from tantalum atoms (Figure S15).

Bader charges quantify the transferred electronic charge.<sup>[45–46]</sup> Based on an idealized structure model of  $\text{PTa}_8\text{N}_{13}$  without mixed occupancies, the cation sites exhibit values from +2.07e to +2.30e (Ta) and +2.83e (P), whereas values for all N atoms range from –1.49e to –1.65e. This indicates charge transfer from Ta/P to N.

The values are comparable to those calculated for a group of known tantalum nitrides (Figure 4b<sup>[7,14,16–18,47–49]</sup>). Bader charges for tantalum nitrides with  $\text{Ta}^{+V}$  and  $\text{Ta}^{+III}$  typically range from 2.27e to 2.67e ( $\text{HP-Ta}_3\text{N}_5$ ,  $\text{Ta}_3\text{N}_5$ ,  $\delta$ -TaON) and from 1.57e to 1.94e ( $\theta$ -,  $\delta$ -TaN), respectively.  $\text{Ta}_2\text{N}_3$  has been described with Ta in the formal oxidation states of +4.56(5) and +4.47(5),<sup>[17]</sup> and Bader charges ranging from 2.20e to 2.31e.  $\varepsilon$ -TaN exhibits a wider range of Bader charges for atoms with predominantly metallic (0.80e) to rather ionic (2.23e) bonds. All Ta atoms in  $\text{P}_{1-x}\text{Ta}_{8+x}\text{N}_{13}$  ( $x=0.1–0.15$ ) experience almost the same electronic environment. The Bader charges are close to values for +4.5 and +5, all Bader charges and valence electron values are given in Tables S8.

Density functional theory (DFT) calculations for idealized  $\text{PTa}_8\text{N}_{13}$  yield a total DOS (Figure 4c) and partial DOS values for all atom types (Figures S17–19). The valence band ranges from –12 to 0 eV and consists mainly of nitrogen sites with *p* character and tantalum sites with *d* character. The fraction of phosphorus states in the total DOS is low and *s*, *p*, and *d* states of phosphorus mix within the valence band.  $\text{PTa}_8\text{N}_{13}$  shows predominantly ionic bonding between phosphorus and nitrogen atoms. The *p* and *d* states of P are degenerate, and the *p* valence bands of the nitrogen atoms N1 and N7 contain significantly more electronic states, indicating electron localization near the N atoms. The bonds between tantalum and nitrogen atoms (N2/N4–N6) exhibit a combination of ionic and covalent properties. The *p* valence bands of N2/N4–N6 have more electronic states than the *d* bands of the tantalum atoms, and these are degenerate across the valence band, as well. Interactions between Ta2/3 and N3 form predominantly covalent bonds, as the *d* valence bands of the tantalum have similar electronic states to the *p* valence band of nitrogen N3. The powder sample has a dark optical appearance that matches the *d* states of tantalum at the Fermi energy. Additionally, the calculations result in states of an interstitial region that cannot be decomposed into orbital-like bands. Calculations of the electron localization function (ELF) support the conclusions from the DOS. The ELF reveals that some valence electrons,

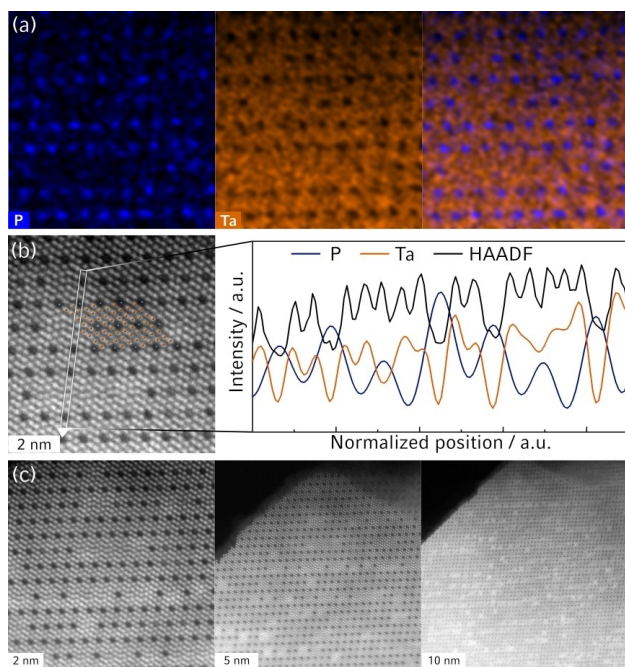


**Figure 3.** STEM-HAADF of  $\text{P}_{1-x}\text{Ta}_{8+x}\text{N}_{13}$  ( $x=0.1–0.15$ ) along [010]; (a) atomic resolution EDX map for P (blue), Ta (orange), and combined map; (b) STEM-HAADF image with structure overlay (left) and a combined line scan of the STEM-HAADF signal with EDX signal. Different intensities correspond to different occupancies of atom columns by Ta and P atoms. Areas with high intensity give a Ta signal in the map and areas with low intensity exhibit a P signal; (c) different magnifications. More details and enlarged versions are given in Figures S8–S11.

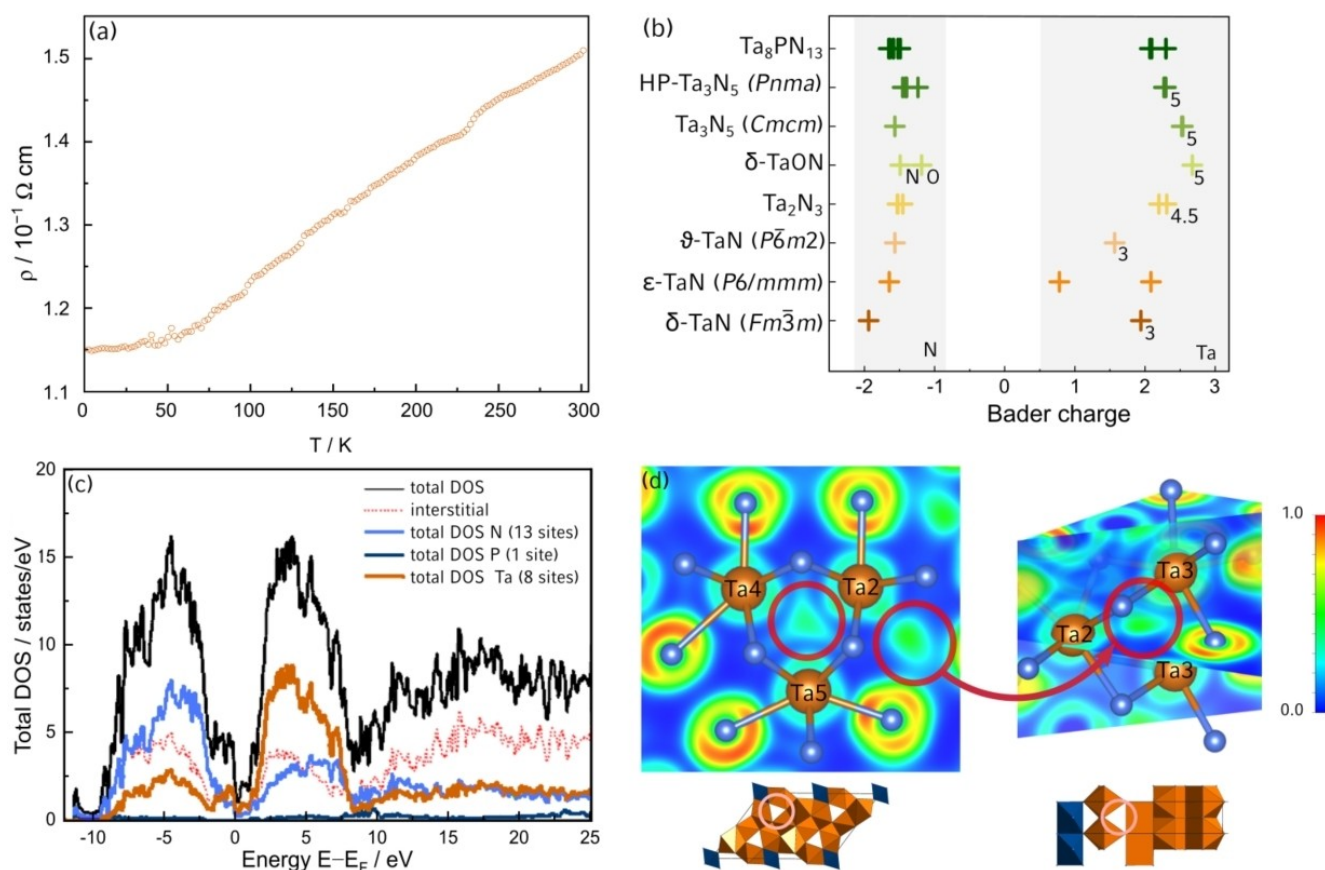


**Figure 4.** (a) Temperature dependence of the electrical resistivity of  $\text{P}_{1-x}\text{Ta}_{8+x}\text{N}_{13}$  ( $x=0.1-0.15$ ); (b) Bader charges of atoms in  $\text{PTa}_8\text{N}_{13}$  compared to tantalum (oxo)nitrides from literature; (c) Total DOS of  $\text{PTa}_8\text{N}_{13}$ . The valence band consists mainly of N atom  $p$  states and Ta atom  $d$  states,  $d$  states of Ta cross  $E_F$ ; the total DOS from  $-40$  to  $25$  eV is given in Figure S16; (d) ELF isosurfaces display paired electron density located between groups of three Ta atoms inside small channels (left) and voids of the structure (right), Ta: orange, N: light blue,  $\text{PN}_6$  octahedra: dark blue.

presumably of tantalum, are not participating in Ta–N bonds. Instead, some paired electron density is concentrated between clusters of three tantalum atoms in two spatial orientations: The electrons are localized in small channels (Figure 4d left) and in small vacant regions in the structure (Figure 4d right).

To summarize,  $\text{P}_{1-x}\text{Ta}_{8+x}\text{N}_{13}$  ( $x=0.1-0.15$ ) stands out as the first ternary transition metal nitride containing phosphorus. The synthesis via a high-pressure, high-temperature approach, the structural elucidation as well as the magnetic and electric properties give a consistent picture of structure and bonding. The condensed tantalum nitride network incorporates edge-sharing  $\text{PN}_6$  octahedra. Electron microscopy directly illustrates the P/Ta disorder. Both experimental data and DFT calculations indicate positive polarized Ta atoms with very similar electronic environments for all coordination states.  $\text{P}_{1-x}\text{Ta}_{8+x}\text{N}_{13}$  serves as a model structure with a bonding situation that features both, covalent and metallic character. This enables the exploration of unconventional physical properties, such as high resistivity with metallic character.

## Supporting Information

The authors have cited additional references within the Supporting Information.<sup>[50–90]</sup>

Deposition number 2345638 contains the supplementary crystallographic data for this paper. These data are provided free of charge by the joint Cambridge Crystallographic Data Centre and Fachinformationszentrum Karlsruhe Access Structures service.

## Acknowledgements

We thank Amalina Buda and Dominik Werhahn (Department of Chemistry at LMU Munich) for SEM investigations and preliminary susceptibility measurements. We thank Dr. Katherine R. Fisher for the electron paramagnetic resonance data. The authors acknowledge funding support from the Deutsche Forschungsgemeinschaft (DFG, German Research Foundation) under Germany's Excellence Strategy-EXC 2089/1-390776260 (e-Conversion) as well as the projects SCHN 377/18-1 and OE 530/6-1. Furthermore, we thank the Natural Sciences and Engineering Research Council of Canada (NSERC) and the Canada Research

Chair program for their financial support. We also thank the Graham HPC cluster and the Digital Research Alliance of Canada for providing computing resources. Open Access funding enabled and organized by Projekt DEAL.

### Conflict of Interest

The authors declare no conflict of interest.

### Data Availability Statement

The data that support the findings of this study are available in the supplementary material of this article.

**Keywords:** disorder · electron microscopy · high-pressure chemistry · nitrides · structure elucidation

- [1] Y. Zhong, X. Xia, F. Shi, J. Zhan, J. Tu, H. J. Fan, *Adv. Sci.* **2016**, *3*, 1500286.
- [2] A. L. Greenaway, C. L. Melamed, M. B. Tellekamp, R. Woods-Robinson, E. S. Toberer, J. R. Neilson, A. C. Tamboli, *Annu. Rev. Mater. Res.* **2021**, *51*, 591–618.
- [3] Y. Xiao, C. Feng, J. Fu, F. Wang, C. Li, V. F. Kunzelmann, C.-M. Jiang, M. Nakabayashi, N. Shibata, I. D. Sharp, *Nat. Catal.* **2020**, *3*, 932–940.
- [4] C.-M. Jiang, L. I. Wagner, M. K. Horton, J. Eichhorn, T. Rieth, V. F. Kunzelmann, M. Kraut, Y. Li, K. A. Persson, I. D. Sharp, *Mater. Horiz.* **2021**, *8*, 1744–1755.
- [5] F. S. Hegner, A. Cohen, S. S. Rudel, S. Kronawitter, M. Grumet, X. Zhu, R. Korobko, L. Houben, C.-M. Jiang, W. Schnick, G. Kieslich, O. Yaffe, I. D. Sharp, D. A. Egger, *Adv. Energy Mater.* **2024**, *14*, 2303059.
- [6] G. Brauer, W. Kiliani, *Z. Anorg. Allg. Chem.* **1979**, *452*, 17–26.
- [7] N. Terao, *Jpn. J. Appl. Phys.* **1971**, *10*, 248–259.
- [8] L. Conroy, A. N. Christensen, *J. Solid State Chem.* **1977**, *20*, 205–207.
- [9] N. Schönberg, W. Overend, A. Munthe-Kaas, N. A. Sørensen, *Acta Chem. Scand.* **1954**, *8*, 1217–1221.
- [10] G. Brauer, K. H. Zapp, *Z. Anorg. Allg. Chem.* **1954**, *277*, 129–139.
- [11] A. N. Christensen, B. Lebeck, *Acta Crystallogr. Sect. B* **1978**, *34*, 261–263.
- [12] J. Gatterer, G. Dufek, P. Etmayer, R. Kieffer, *Monatsh. Chem.* **1975**, *106*, 1137–1147.
- [13] T. Mashimo, S. Tashiro, T. Toya, M. Nishida, H. Yamazaki, S. Yamaya, K. Oh-Ishi, Y. Syono, *J. Mater. Sci.* **1993**, *28*, 3439–3443.
- [14] G. Brauer, E. Mohr, A. Neuhaus, A. Skokan, *Monatsh. Chem.* **1972**, *103*, 794–798.
- [15] T. Mashimo, S. Tashiro, *J. Mater. Sci. Lett.* **1994**, *13*, 174–176.
- [16] A. Y. Ganin, L. Kienle, G. V. Vajenine, *Eur. J. Inorg. Chem.* **2004**, *2004*, 3233–3239.
- [17] A. Zerr, G. Miehe, J. Li, D. A. Dzivenko, V. K. Bulatov, H. Höfer, N. Bolfan-Casanova, M. Fialin, G. Brey, T. Watanabe, *Adv. Funct. Mater.* **2009**, *19*, 2282–2288.
- [18] N. E. Brese, M. O’Keeffe, P. Rauch, F. J. DiSalvo, *Acta Crystallogr. Sect. C* **1991**, *47*, 2291–2294.
- [19] H. Alkhalidi, P. Kroll, *J. Phys. Chem. C* **2020**, *124*, 22221–22227.
- [20] R. Niewa, D. A. Zherebtsov, H. Borrmann, R. Kniep, *Z. Anorg. Allg. Chem.* **2002**, *628*, 2505–2508.
- [21] C. Wachsmann, H. Jacobs, *J. Alloys Compd.* **1992**, *190*, 113–116.
- [22] P. Höhn, R. Kniep, J. Maier, *Angew. Chem. Int. Ed.* **1993**, *9*, 1350–1352.
- [23] F. K.-J. Helmlinger, P. Höhn, R. Kniep, *Z. Naturforsch. B* **1993**, *48*, 1015–1018.
- [24] H. Jacobs, E. von Pinkowski, *J. Less-Common Met.* **1989**, *146*, 147–160.
- [25] T. Brokamp, H. Jacobs, *J. Alloys Compd.* **1992**, *183*, 325–344.
- [26] S. Clarke, F. DiSalvo, *J. Solid State Chem.* **1997**, *132*, 394–398.
- [27] H. Holleck, F. Thümmel, *Monatsh. Chem.* **1967**, *98*, 133–134.
- [28] U. Zachwieja, H. Jacobs, *Eur. J. Solid State Inorg. Chem.* **1991**, *28*, 1055–1062.
- [29] R. Trócoli, C. Frontera, J. Oró-Solé, C. Ritter, P. Alemany, E. Canadell, M. R. Palacín, J. Fontcuberta, A. Fuertes, *Chem. Mater.* **2022**, *34*, 6098–6107.
- [30] R. Niewa, D. A. Zherebtsov, W. Schnelle, F. R. Wagner, *Inorg. Chem.* **2004**, *43*, 6188–6194.
- [31] L. Cario, Z. A. Gál, T. P. Braun, F. J. DiSalvo, B. Blaschkowski, H. J. Meyer, *J. Solid State Chem.* **2001**, *162*, 90–95.
- [32] N. E. Brese, F. J. DiSalvo, *J. Solid State Chem.* **1995**, *120*, 378–380.
- [33] W. Jeitschko, H. Nowotny, F. Benesovsky, *Monatsh. Chem.* **1964**, *95*, 1242–1246.
- [34] G. Brauer, R. Lesser, *Int. J. Mater. Res.* **1959**, *50*, 512–515.
- [35] L. Eisenburger, V. Weippert, C. Paulmann, D. Johrendt, O. Oeckler, W. Schnick, *Angew. Chem. Int. Ed.* **2022**, *61*, e202202014.
- [36] S. D. Kloß, O. Janka, T. Block, R. Pöttgen, R. Glaum, W. Schnick, *Angew. Chem. Int. Ed.* **2019**, *58*, 4685–4689.
- [37] S. Vogel, M. Bykov, E. Bykova, S. Wendl, S. D. Kloß, A. Pakhomova, N. Dubrovinskaia, L. Dubrovinsky, W. Schnick, *Angew. Chem. Int. Ed.* **2020**, *59*, 2730–2734.
- [38] D. Laniel, F. Trybel, A. Néri, Y. Yin, A. Aslandukov, T. Fedotenko, S. Khandarkhaeva, F. Tasnádi, S. Chariton, C. Giacobbe, *Chem. Eur. J.* **2022**, *28*, e202201998.
- [39] S. Vogel, M. Bykov, E. Bykova, S. Wendl, S. D. Kloß, A. Pakhomova, S. Chariton, E. Koemets, N. Dubrovinskaia, L. Dubrovinsky, *Angew. Chem. Int. Ed.* **2019**, *58*, 9060–9063.
- [40] J. Wang, J. Jiang, J. Chen, Y. Li, A. Ma, *Comput. Mater. Sci.* **2018**, *143*, 368–373.
- [41] S. J. Henderson, A. L. Hector, *J. Solid State Chem.* **2006**, *179*, 3518–3524.
- [42] R. D. Shannon, *Acta Crystallogr. Sect. A* **1976**, *32*, 751–767.
- [43] S. Pennycook, *Annu. Rev. Mater. Sci.* **1992**, *22*, 171–195.
- [44] P. Hagemuller, *Prog. Solid State Chem.* **1971**, *5*, 71–144.
- [45] G. Henkelman, A. Arnaldsson, H. Jónsson, *Comput. Mater. Sci.* **2006**, *36*, 354–360.
- [46] R. Bader, W. H. Henneker, P. E. Cade, *J. Chem. Phys.* **1967**, *46*, 3341–3363.
- [47] A. Salamat, K. Woodhead, S. I. U. Shah, A. L. Hector, P. F. McMillan, *Chem. Commun.* **2014**, *50*, 10041–10044.
- [48] T. Lüdtke, A. Schmidt, C. Göbel, A. Fischer, N. Becker, C. Reimann, T. Bredow, R. Dronskowski, M. Lerch, *Inorg. Chem.* **2014**, *53*, 11691–11698.
- [49] M. Grumski, P. P. Dholabhai, J. B. Adams, *Acta Mater.* **2013**, *61*, 3799–3807.
- [50] A. Stock, H. Grüneberg, *Ber. Dtsch. Chem. Ges.* **1907**, *40*, 2573–2578.
- [51] G. Brauer, J. Weidlein, J. Strähle, *Z. Anorg. Allg. Chem.* **1966**, *348*, 298–308.
- [52] D. Rubie, *Phase Transitions* **1999**, *68*, 431–451.
- [53] D. Walker, *Am. Mineral.* **1991**, *76*, 1092–1100.
- [54] D. Walker, M. Carpenter, C. Hitch, *Am. Mineral.* **1990**, *75*, 1020–1028.
- [55] H. Huppertz, *Z. Kristallogr.* **2004**, *219*, 330–338.
- [56] H. M. Rietveld, *J. Appl. Crystallogr.* **1969**, *2*, 65–71.

- [57] A. Coelho, TOPAS Academic, version 6.1 **2007**.
- [58] A. Inc, APEX3, version 2016.5-0, Karlsruhe (Germany) **2001**.
- [59] G. M. Sheldrick, *Acta Crystallogr. Sect. C* **2015**, *71*, 3–8.
- [60] C. B. Hübschle, G. M. Sheldrick, B. Dittrich, *J. Appl. Crystallogr.* **2011**, *44*, 1281–1284.
- [61] DigitalMicrograph, Gatan, version 3.6.5, Pleasanton, California **1999**.
- [62] J. L. Lábár, *Ultramicroscopy* **2005**, *103*, 237–249.
- [63] P. A. Stadelmann, *Ultramicroscopy* **1987**, *21*, 131–145.
- [64] Thermo Fisher Scientific, Velox, version 3, Waltham, Massachusetts **2021**.
- [65] Quantum Design Inc., version 1.5.11 ed., San Diego **2013**.
- [66] K. Schwarz, P. Blaha, G. K. H. Madsen, *Comput. Phys. Commun.* **2002**, *147*, 71–76.
- [67] K. Schwarz, *J. Solid State Chem.* **2003**, *176*, 319–328.
- [68] P. Blaha, K. Schwarz, F. Tran, R. Laskowski, G. K. H. Madsen, L. D. Marks, *J. Chem. Phys.* **2020**, 074101.
- [69] K. Schwarz, P. Blaha, S. B. Trickey, *Mol. Phys.* **2010**, *108*, 3147–3166.
- [70] J. O. Dimmock, in *Solid State Phys.*, vol. 26 (Eds.: H. Ehrenreich, F. Seitz, D. Turnbull), Elsevier **1971**, pp 103–274.
- [71] O. K. Andersen, *Phys. Rev. B* **1975**, *12*, 3060–3083.
- [72] D. D. Koelling, G. O. Arbman, *J. Phys. F* **1975**, *5*, 2041–2054.
- [73] E. Sjöstedt, L. Nordström, D. J. Singh, *Solid State Commun.* **2000**, *114*, 15–20.
- [74] G. K. H. Madsen, P. Blaha, K. Schwarz, E. Sjöstedt, L. Nordström, *Phys. Rev. B* **2001**, *64*, 195134.
- [75] J. P. Perdew, K. Burke, M. Ernzerhof, *Phys. Rev. Lett.* **1996**, *77*, 3865–3868.
- [76] F. Tran, P. Blaha, K. Schwarz, P. Novák, *Phys. Rev. B* **2006**, *74*, 155108.
- [77] F. Tran, P. Blaha, *Phys. Rev. B* **2011**, *83*, 235118.
- [78] G. Kresse, J. Hafner, *Phys. Rev. B* **1993**, *47*, 558–561.
- [79] G. Kresse, J. Hafner, *Phys. Rev. B* **1994**, *49*, 14251–14269.
- [80] G. Kresse, J. Furthmüller, *Comput. Mater. Sci.* **1996**, *6*, 15–50.
- [81] G. Kresse, J. Furthmüller, *Phys. Rev. B* **1996**, *54*, 11169–11186.
- [82] G. Kresse, D. Joubert, *Phys. Rev. B* **1999**, *59*, 1758–1775.
- [83] P. E. Blöchl, *Phys. Rev. B* **1994**, *50*, 17953–17979.
- [84] H. J. Monkhorst, J. D. Pack, *Phys. Rev. B* **1976**, *13*, 5188–5192.
- [85] W. H. Press, B. P. Flannery, S. A. Teukolsky, W. T. Vetterling, *Numerical Recipes*, Cambridge Univ. Press, New York **1986**.
- [86] B. Silvi, A. Savin, *Nature* **1994**, *371*, 683–686.
- [87] R. F. Bader, *Acc. Chem. Res.* **1985**, *18*, 9–15.
- [88] G. Henkelman, A. Arnaldsson, H. Jónsson, *Comput. Mater. Sci.* **2006**, *36*, 354–360.
- [89] A. Salamat, K. Woodhead, S. I. U. Shah, A. L. Hector, P. F. McMillan, *Chem. Commun.* **2014**, *50*, 10041–10044.
- [90] M. Grumski, P. P. Dholabhai, J. B. Adams, *Acta Mater.* **2013**, *61*, 3799–3807.

Manuscript received: June 18, 2024

Accepted manuscript online: July 23, 2024

Version of record online: September 12, 2024